UCRL-JRNL-217882

Relativistic multireference many-body perturbation theory calculations on F-, Ne-, Na-, Mg-, Al-, Si-, and P-like xenon ions

M. J. Vilkas, Y. Ishikawa, E. Träbert

December 27, 2005

Journal of Physics B

Relativistic multireference many-body perturbation theory calculations on F-, Ne-, Na-, Mg-, Al-, Si- and P-like xenon ions

Marius J. Vilkas†, Yasuyuki Ishikawa† and Elmar Träbert‡

† Department of Chemistry, University of Puerto Rico, P.O. Box 23346 San Juan, Puerto Rico 00931-3346 USA

‡ Experimentalphysik III, Ruhr-Universität Bochum, D-44780 Bochum, Germany, and High Temperature and Astrophysics Division, LLNL, P.O. Box 808, Livermore, CA 94550, U.S.A.

E-mail: traebert@ep3.rub.de

Abstract. Many-Body Perturbation Theory (MBPT) has been employed to calculate with high wavelength accuracy the extreme ultraviolet (EUV) spectra of F-like to P-like Xe ions. We discuss the reliability of the new calculations using the example of EUV beam-foil spectra of Xe, in which n=3, Δn=0 transitions of Na-, Mg-, Al-like, and Si-like ions have been found to dominate. A further comparison is made with spectra from an electron beam ion trap, that is, from a device with a very different (low density) excitation balance.

PACS numbers: 3270Jc, 3115Md, 3450Fa

to be Submitted to: *J. Phys. B: At. Mol. Opt. Phys.*

1. Introduction

Surveys of the data holdings of, for example, the NIST atomic spectra data base [1] show how only for elements up to about Z=28 (Ni) there are at least some data for practically all charge states (though often deplorably incomplete). With the exception of some elements that are of interest in fusion energy research, data for most heavier elements are largely limited to neutral atoms and the first few ionization stages, to calculated values for one- and two-electron ions, and to the resonance lines of ions with a single valence electron (Na-like, Cu-like). The general character of spectra of any ion species can nowadays be quickly derived from calculations. However, most of these calculations fall far short of spectroscopic accuracy. If an experimental spectrum was to show a few hundred lines, and theory predicted a few hundred lines, there would be no easy mapping of one set to the other, and most likely it would turn out (as it regularly does) that the experiment shows a plenitude of lines that are not identifiable

from current calculations. As an example, we cite the long-drawn and not yet fully successful quest for the analysis of beam-foil spectra of four- to six-electron ions of an element as light as Ne (Z=10) [2, 3, 4, 5, 6]. It would be a mark of substantial progress if even the most prominent lines in spectra of ions with two to four valence electrons could be predicted well enough to enable immediate identification within the experimental and calculational uncertainties.

Of course, most calculations can be adjusted to some experimental atomic structure parameters, and such scaled calculations can then predict further atomic data with improved reliability. A test that precludes such a bias would require uncharted experimental data and unadjusted, that is, *ab initio* calculations. We resort to experimental data for atomic systems well beyond the bulk of well-analyzed spectra, and thus with some uncertainty in the earlier line classifications. The data are from a series of beam-foil experiments on Xe and Au [7, 8, 9] that have, about a decade ago, pushed the envelope of such enterprises. (One of us, E.T., was the lead author of those three studies, and some of the laboratory notes and other unpublished material of the time are available to us for a re-investigation.) In the present paper we concentrate on the Xe data which are not as far beyond well-charted territory as are the Au data (which will be discussed elsewhere, eventually). We also compare our results to Xe spectra recently obtained at the Livermore electron beam ion trap SuperEBIT [10], that is, a light source with very different excitation conditions; those spectra are of much higher spectral resolution than the earlier beam-foil spectra. There is very little other experimental information on the EUV spectra of such highly charged Xe ions as we discuss, and most of that [11, 12, 13] is on n = 2 - 3 transitions in Ne-like ions which we do not cover. Xe has recently found interest in the context of developing a light source for EUV lithography; the charge states needed to produce light at 135 Å are much lower though than the ones discussed here (about q=8+ vs. q=39+ to q=45+). Intermediate to these two ranges of charge states are investigations of EUV light emission from a low-inductance vacuum spark [14], after electron capture by Xe ions of q= 8+ to 16+ from He gas [15], and studies at the Berlin EBIT [16] of EUV spectra of Xe^{17+} to Xe^{25+}.

We apply our Multi-Reference Møller-Plesset calculations to determine levels and transition probabilities in F- to P-like ions of Xe and to obtain theoretical predictions of a multitude of prominent transitions in the spectral range of the observations. We simulate spectra for a visual comparison with the available data. It turns out that such calculations alleviate the calibration problem in the beam-foil data, largely explain even minor features in the observed spectra, and appear to be eminently useful guides for future experiments.

2. Theory

The effective N-electron Hamiltonian (in atomic units) for the development of our relativistic MR-MP algorithm is taken to be the relativistic "no-pair" Dirac-Coulomb-

Breit (DCB) Hamiltonian [17, 18]

$$H^{+}_{DCB} = \sum_i h_D(i) + \mathcal{L}_+ \left(\sum_{i>j} \frac{1}{r_{ij}} + B_{ij}(0) \right) \mathcal{L}_+ \tag{1}$$

with

$$B_{ij}(0) = -\frac{1}{2}[\boldsymbol{\alpha}_{\ i} \cdot \boldsymbol{\alpha}_{\ j} + (\boldsymbol{\alpha}_{\ i} \cdot \mathbf{r}_{ij})(\boldsymbol{\alpha}_{\ j} \cdot \mathbf{r}_{ij})/r^2_{ij}]/r_{ij}, \tag{2}$$

Here $h_D(i)$ is the Dirac one-electron Hamiltonian. The DCB Hamiltonian is covariant to first order and increases the accuracy of calculated fine-structure splittings and inner-shell binding energies. Higher order QED effects appear first in order α^3. The nucleus is modeled as a sphere of uniform proton charge distribution. $\mathcal{L}_+ = L_+(1)L_+(2)\ldots L_+(N)$, where $L_+(i)$ is the projection operator onto the space $D^{(+)}$ spanned by the positive-energy eigenfunctions of the matrix Dirac-Fock-Breit (DFB) SCF equation [18]. $\mathcal{L}_+$ is the projection operator onto the positive-energy space $\mathfrak{D}^{(+)}$ spanned by the N-electron configuration-state functions (CSF) constructed from the positive-energy eigenfunctions of the matrix DFB SCF. It takes into account the field-theoretic condition that the negative-energy states are filled. The eigenfunctions $\{\phi^{(\pm)}_{n_q\kappa_q}(r)\}(\in\ D^{(+)} \cup D^{(-)})$ of the matrix DFB SCF equation clearly separate into two discrete manifolds, $D^{(+)}$ and $D^{(-)}$, respectively, of positive- and negative-energy one-particle states. As a result, the positive-energy projection operators can be accomodated easily in many-body calculations. The formal conditions on the projection are automatically satisfied when only the positive-energy spinors are employed.

N-electron eigenfunctions of the no-pair DCB Hamiltonian are approximated by a linear combination of M_{MC} configuration-state functions, $\{\Phi^{(+)}_I(\gamma_I\mathcal{J}\pi); I = 1,2,\ldots,M_{MC}\}\in\ \mathfrak{P}^{(+)}$, constructed from positive-energy eigenfunctions of the matrix multiconfiguration Dirac-Fock-Breit (MCDFB) SCF equation,

$$\psi^{MC}_{K}(\gamma_K\mathcal{J}\pi) = \sum_{I}^{M_{MC}} C_{IK}\Phi^{(+)}_I(\gamma_I\mathcal{J}\pi). \tag{3}$$

The MCDFB SCF wave function $\psi^{MC}_{K}(\gamma_K\mathcal{J}\pi)$ is an eigenfunction of the angular momentum and parity operators with total angular momentum $\mathcal{J}$ and parity π. γ denotes a set of quantum numbers other than $\mathcal{J}$ and π necessary to specify the state uniquely. The total DCB energy of the general state represented by the MC wave function $\psi^{MC}_{K}(\gamma_K\mathcal{J}\pi)$ can be expressed as

$$E^{MC}_{DCB}(\gamma_K\mathcal{J}\pi) = \sum_{IJ}^{\mathfrak{P}(+)} C_{IK}C_{JK} < \Phi^{(+)}_I(\gamma_I\mathcal{J}\pi)|H^{+}_{DCB}|\Phi^{(+)}_J(\gamma_J\mathcal{J}\pi) > \tag{4}$$

Here, it is assumed that $\psi_K(\gamma_K\mathcal{J}\pi)$ and $\Phi^{(+)}_J(\gamma_J\mathcal{J}\pi)$ are normalized.

Second-order variation of the state-averaged energy $\Omega_{state-ave}$ given below is taken with respect to the matrix elements of spinor unitary rotation matrix and configuration mixing coefficients $\{C_{IK}\}$, leading to the Newton-Raphson equations for second-order

MCDFB SCF [19]. This state-averaged second-order MCDFB equations yields a single set of spinors for the ground and low-lying even- and odd-parity excited (γ,$\mathcal{J}$,π) levels.

$$\Omega_{state-ave} = \sum_{\gamma_K \mathcal{J}\pi} E^{MC}_{DCB}(\gamma_K \mathcal{J}\pi) =$$

$$\sum_{\gamma_K \mathcal{J}\pi} \sum_{IJ}^{\mathfrak{P}(+)} C_{IK} C_{JK} < \Phi^{(+)}_I(\gamma_I \mathcal{J}\pi) | H^{+}_{DCB} | \Phi^{(+)}_J(\gamma_J \mathcal{J}\pi) > \tag{5}$$

where summation indices, γ ,$\mathcal{J}$, and π, run over the ground and excited states.

In order to account for strong configuration mixing among the highly excited levels, the multireference configuration interaction method (MR-CI) [20] is introduced in an extended subspace $\mathfrak{P}^{(+)}_{CI}$ of positive-energy space. N-electron eigenfunctions of the no-pair DCB Hamiltonian are approximated by a linear combination of $M_{CI}(>> M_{MC})$ configuration-state functions, $\{\Phi^{(+)}_I(\gamma_I \mathcal{J}\pi); I = 1, 2, \ldots, M_{CI}\}$, constructed from the one-particle positive-energy spinors computed in matrix MCDFB SCF. Variation of the configuration-state coefficients $\{C_{IK}\}$ leads to the determinantal CI equation.

$$\det(\langle \Phi^{(+)}_I(\gamma_I \mathcal{J}\pi) \mid H^{+}_{DCB} \mid \Phi^{(+)}_J(\gamma_J \mathcal{J}\pi)\rangle -$$

$$E^{CI} \langle \Phi^{(+)}_I(\gamma_I \mathcal{J}\pi) \mid \Phi^{(+)}_J(\gamma_J \mathcal{J}\pi)\rangle) = 0 \tag{6}$$

The eigenfunctions $\{\psi^{CI}_K(\gamma_K \mathcal{J}\pi)\}$ form a subspace $\mathfrak{P}^{(+)}_{CI}$ of the positive-energy space $\mathfrak{D}^{(+)}$.

$$\psi^{CI}_K(\gamma_K \mathcal{J}\pi) = \sum_{I}^{M_{CI}} C_{IK} \Phi^{(+)}_I(\gamma_I \mathcal{J}\pi), \; K = 1, 2, ..M_{CI}. \tag{7}$$

The total DCB energy of the general CI state $|\psi^{CI}_K(\gamma_K \mathcal{J}\pi) >$ can be expressed as

$$E^{CI}_K(\gamma_K \mathcal{J}\pi) =< \psi^{CI}_K(\gamma_K \mathcal{J}\pi) | H^{+}_{DCB} | \psi^{CI}_K(\gamma_K \mathcal{J}\pi) >=$$

$$= \sum_{I,J=1}^{\mathfrak{P}_{CI}(+)} C_{IK} C_{JK} < \Phi^{(+)}_I(\gamma_I \mathcal{J}\pi) | H^{+}_{DCB} | \Phi^{(+)}_J(\gamma_J \mathcal{J}\pi) > . \tag{8}$$

Here it is assumed that $\psi^{CI}_K(\gamma_K \mathcal{J}\pi)$ and $\Phi^{(+)}_I(\gamma_I \mathcal{J}\pi)$ are normalized.

The frequency-dependent Breit interaction, normal mass shift (NMS) and specific mass shift (SMS) are evaluated as the first-order corrections using the eigenvectors $\{\psi^{CI}_K(\gamma_K \mathcal{J}\pi)\}$ from the MR-CI.

$$< \psi^{CI}_K(\gamma_K \mathcal{J}\pi) | \Delta B(\omega) + H_{NMS} + H_{SMS} | \psi^{CI}_K(\gamma_K \mathcal{J}\pi) > \tag{9}$$

Here the frequency-dependent Breit interaction, $\Delta B(\omega)$, and normal and specific mass shift operators are given by

$$\Delta B(\omega) = \sum_{i>j} [- \frac{\boldsymbol{\alpha}_i \cdot \boldsymbol{\alpha}_j}{r_{ij}} \cos(\omega r_{ij}) +$$

$$(\boldsymbol{\alpha}_i \cdot \boldsymbol{\nabla}_i)(\boldsymbol{\alpha}_j \cdot \boldsymbol{\nabla}_j)(\cos(\omega r_{ij}) - 1)/(\omega^2 r_{ij}) - B_{ij}(0)], \tag{10}$$

$$H_{NMS} = \frac{1}{2M} \sum_i \boldsymbol{p}_i^{\,2}, \tag{11}$$

and

$$H_{SMS} = \frac{1}{M} \sum_{i>j} (\boldsymbol{p}_i \cdot \boldsymbol{p}_j), \tag{12}$$

where M is the nuclear mass. The frequency dependence of the Breit interaction is evaluated in the Coulomb gauge, subtracting frequency-independent Breit interaction which is already included ($B^{(0+1)}(0)$) in MR-CI (Eq. 8). The first-order corrections calculated in this way are denoted $\Delta B^{(1)}(\omega)$.

The no-pair DCB Hamiltonian H^+_{DCB} is decomposed into two parts, unperturbed Hamiltonian H_0 and perturbation V, following Møller and Plesset [21],

$$H^+_{DCB} = H_0 + V, \tag{13}$$

$$H_0 = \sum_I^{\mathfrak{D}(+)} |\Phi_I^{(+)}(\gamma_I \mathcal{J}\pi) > E_I^{CSF} < \Phi_I^{(+)}(\gamma_I \mathcal{J}\pi)|, \tag{14}$$

so that

$$H_0 |\Phi_I^{(+)}(\gamma_I \mathcal{J}\pi) >= E_I^{CSF} |\Phi_I^{(+)}(\gamma_I \mathcal{J}\pi) > (I = 1, 2, \ldots). \tag{15}$$

E_I^{CSF} is a sum of the products of one-electron energies defined by ε_q^+ and an occupation number $n_{n_q\kappa_q}[I]$ of the κ_q-symmetry shell in the CSF $\Phi_I^{(+)}(\gamma_I \mathcal{J}\pi)$ [22, 23];

$$E_I^{CSF} = \sum_q^{D(+)} \varepsilon_q^+ n_{n_q\kappa_q}[I]. \tag{16}$$

The subset, $\{\Phi_I^{(+)}(\gamma_I \mathcal{J}\pi); I = 1, 2, \ldots, M_{CI}\}$, with which we expand the CI wavefunction $\psi_K^{CI}(\gamma_K \mathcal{J}\pi)$ (Eq. 7) defines an active subspace $\mathfrak{P}_{CI}^{(+)}$ spanned by $\psi_K^{CI}(\gamma_K \mathcal{J}\pi)$ and its $M_{CI} - 1$ orthogonal complements, $\{\psi_K(\gamma_K \mathcal{J}\pi); K = 1, 2, \ldots, M_{CI}\}$. The matrix of H^+_{DCB} in this subspace is diagonal

$$< \psi_K^{CI}(\gamma_K \mathcal{J}\pi) | H^+_{DCB} | \psi_L^{CI}(\gamma_L \mathcal{J}\pi) >= \delta_{KL} \left(E_K^{(0)} + E_K^{(1)} \right) =$$

$$\delta_{KL} E_K^{CI}(\gamma_K \mathcal{J}\pi), \tag{17}$$

where

$$E_K^{(0)} =< \psi_K^{CI}(\gamma_K \mathcal{J}\pi) | H_0 | \psi_K^{CI}(\gamma_K \mathcal{J}\pi) >= \sum_I^M C_{IK} C_{IK} E_I^{CSF} \tag{18}$$

and

$$E_K^{(1)} =< \psi_K^{CI}(\gamma_K \mathcal{J}\pi) | V | \psi_K^{CI}(\gamma_K \mathcal{J}\pi) > . \tag{19}$$

The residual space in the positive-energy subspace is $\mathfrak{Q}^{(+)} = \mathfrak{D}^{(+)} - \mathfrak{P}_{CI}^{(+)}$, which is spanned by CSFs $\{\Phi_I^{(+)}(\gamma_I \mathcal{J}\pi); I = M_{CI} + 1, M_{CI} + 2, \ldots\}$.

Application of Rayleigh-Schrödinger perturbation theory provides order-by-order expressions of the perturbation series for the state approximated by $|\psi_K^{CI}(\gamma_K \mathcal{J}\pi)>$,

$$E_K(\gamma_K \mathcal{J}\pi) = E_K^{CI}(\gamma_K \mathcal{J}\pi) + E_K^{(2)} + \ldots, \tag{20}$$

where

$$E_K^{(2)} =< \psi_K^{CI}(\gamma_K \mathcal{J}\pi)|V\mathcal{R}V|\psi_K^{CI}(\gamma_K \mathcal{J}\pi) > \tag{21}$$

Here, $\mathcal{R}$ is the resolvent operator,

$$\mathcal{R} = \frac{\mathcal{Q}^{(+)}}{E_K^{CSF} - H_0} \tag{22}$$

with

$$\mathcal{Q}^{(+)} = \sum_I^{\mathfrak{Q}(+)} |\Phi_I^{(+)}(\gamma_I \mathcal{J}\pi) >< \Phi_I^{(+)}(\gamma_I \mathcal{J}\pi)|. \tag{23}$$

The projection operator $\mathcal{Q}^{(+)}$ projects onto the subspace $\mathfrak{Q}^{(+)}$ spanned by CSFs $\{\Phi_I^{(+)}(\gamma_I \mathcal{J}\pi); I = M_{CI}+1, M_{CI}+2, \ldots\}$. Using the spectral resolution of the resolvent operator acting on $V|\Phi_I^{(+)}(\gamma_I \mathcal{J}\pi) >$, the second-order correction may be expressed as,

$$E_K^{(2)} = \sum_{IJ} C_{IK}C_{JK} < \Phi_I^{(+)}(\gamma_I \mathcal{J}\pi)|V\mathcal{R}V|\Phi_J^{(+)}(\gamma_J \mathcal{J}\pi) >=$$

$$= \sum_{L=M+1}^{\mathfrak{Q}(+)} \sum_{I,J=1}^{\mathfrak{P}_{CI}(+)} C_{IK}C_{JK} \frac{< \Phi_I^{(+)}(\gamma_I \mathcal{J}\pi)|V|\Phi_L^{(+)}(\gamma_L \mathcal{J}\pi) >}{E_J^{CSF} - E_L^{CSF}} \cdot$$

$$< \Phi_L^{(+)}(\gamma_L \mathcal{J}\pi)|V|\Phi_J^{(+)}(\gamma_J \mathcal{J}\pi) > . \tag{24}$$

In this form, all perturbation corrections beyond first order describe residual dynamic correlation correction for the state approximated by the CI wavefunction $|\psi_K^{CI}(\gamma_K \mathcal{J}\pi) >$.

Summations over the CSFs in Eqs. (22) and (24) are restricted to CSFs ($\in \mathfrak{D}^{(+)}$) constructed from the positive-energy branch ($D^{(+)}$) of the spinors, effectively incorporating into the computational scheme the "no-pair" projection operator $\mathcal{L}_+$ contained in the DCB Hamiltonians. Further, the CSFs $\Phi_L^{(+)}(\gamma_L \mathcal{J}\pi)$ ($\in \mathfrak{Q}^{(+)}$) generated by excitations higher than double, relative to the reference CSFs $\Phi_I^{(+)}(\gamma_I \mathcal{J}\pi)$ ($\in \mathfrak{P}^{(+)}$), do not contribute to the second- and third-order because for them $< \Phi_I^{(+)}(\gamma_I \mathcal{J}\pi)|V|\Phi_L^{(+)}(\gamma_L \mathcal{J}\pi) >= 0$ and $< \Phi_I^{(+)}(\gamma_I \mathcal{J}\pi)|H_{DCB}^+|\Phi_L^{(+)}(\gamma_L \mathcal{J}\pi) >= 0$. State-specific MR-MP on each of the states obtained in the CI account for both dynamic pair and pair-pair correlations. Consequently, energy converges at the second-order level, yielding highly accurate term energies for a wide range of excited levels.

The large and small radial components of the Dirac spinors are expanded in sets of even-tempered Gaussian-type functions (GTF) that satisfy the boundary conditions associated with the finite nucleus [24]. The speed of light is taken to be 137.0359895 a.u. throughout this study. The GTFs that satisfy the boundary conditions associated with the finite nucleus are automatically kinetically balanced [24]. Even-tempered basis sets

of 26s24p20d18f G spinors (G for "Gaussian") for up to angular momentum L=3 and 15 G spinors for L=4-11 are employed. The order of the partial-wave expansion L_{max}, the highest angular momentum of the spinors included in the virtual space, is L_{max}=11 throughout this study. The nuclei were simulated as spheres of uniform proton charge with the radii $R = A^{1/3}$, where A is atomic mass.

All electrons have been included in the MR-MP perturbation theory calculations to determine accurately the effects of relativity on electron correlation. Radiative corrections, the Lamb shifts, were estimated for each state by evaluating the electron self-energy and vacuum polarization following an approximation scheme discussed by Indelicato, Gorceix, and Desclaux [25]. The code described in Refs. [25] and [26] was adapted to our basis set expansion calculations for this purpose: All the necessary radial integrals were evaluated analytically. In this scheme [26], the screening of the self energy is estimated by integrating the charge density of a spinor to a short distance from the origin, typically 0.3 Compton wavelength. The ratio of the integral computed with an MCDFB SCF spinor and that obtained from the corresponding hydrogenic spinor is used to scale the self-energy correction for a bare nuclear charge that has been computed by Mohr [27].

3. Experimental data

The experimental set-up of the beam-foil work on Xe and Au at the Darmstadt (Germany) GSI UNILAC accelerator has been described elsewhere [7, 8, 9]. This experimental arrangement has gone through various development stages; most of the experimental effort was directed at the precision spectroscopy of few-electron ions, in particular the determination of QED contributions to the transition energies of n=2 - 2 transitions in Li- and Be-like ions [28, 29, 30, 31, 32]. In contrast, the spectral lines of interest in the present study are largely in a spectral range beyond the reach of calibration lines from the stationary calibration light source available. This shortage of external wavelength references necessitated the use of internal ('in-beam') calibration lines, of which there were rather few and far in between, combined with a calculated dispersion curve.

The Xe experiment [7, 8] aimed primarily at spectra from which decay curves of the resonance lines of Na-like Xe ions were to be constructed and then atomic level lifetimes and transition probabilities derived. The wavelengths of the 3s-3p transitions can be calculated well enough for such purpose. Considering the high cost of producing a beam of ions that are fast enough to yield a Na-like charge state fraction after passage through a thin carbon foil, it is advantageous to minimize the data collection time, and to this goal observe the emission spectrum with a multichannel (spatially extended) detector that may record signal for several spectral lines in parallel. Such an arrangement has the added advantage that it is not necessary to preposition the spectrometer to a given exact wavelength including the substantial Doppler correction. If the line of sight of the spectrometer is well determined, then it is even possible to establish a wavelength

calibration with a stationary light source and to transfer the wavelength scale to the observation of fast moving ions via the observation angle and the first and second order Doppler shifts.

For the grazing incidence spectrometer available at GSI (with a R=5 m radius of curvature grating / 5 m diameter Rowland circle), the wavelength calibration was established with the aid of a stationary Penning discharge (with Ne [36], Mg, or Al lines above a wavelength of about 130 Å) and careful angle measurements of the spectrometer, ascertaining that it viewed the ion beam at right angles so that - one hopes - the observed spectral lines are unshifted by the first order Doppler effect, while the correction for the second order (time dilation) was taken from the separately measured beam energy (ion velocity 11.2% of the speed of light, time dilation factor γ= 1.0063). However, the wavelength determination effort was very limited, because the lamp produced lines only near one end of the wavelength range of the EUV observations. Also, the experiment primarily aimed at a determination of transition rates, a goal that required line identification, but not any precise wavelength measurement. Moreover, the type of multichannel detector used is known to be rather linear in position information in the central part, but less so towards the edges. If precise wavelength measurements are being tried with such a detector, widely overlapping, well calibrated spectra are a necessity. Such an approach was not compatible with the time frame of the given experiment.

The spectrometer was equipped with a detector based on microchannel plates and a zig-zag anode read-out. For each wavelength setting, the detector had to be positioned at the Rowland circle, which is a matter of two coordinates and a rotation angle. Such a detector has an efficiency that depends on both the wavelength and the angle under which the photons strike the first surface. Consequently the spectra of adjacent settings seem to make a sawtooth pattern, because there is a slope of the signal across the detector as well as an overall efficiency factor and a possible offset, neither of which has been quantified. The dispersion established in the wavelength range near 130 to 160 Å was used as an approximation throughout, relying on perceived line identifications of n = 3 - 3 transitions in Na-like ions, which can be calculated well, for reference markers in the individual spectral sections imaged on the 40 mm wide position sensitive detector. However, a constant dispersion was a reasonable approximation for only two of the three spectral slices, but not for the third. At short wavelengths, the dispersion (wavelength interval divided by distance along the Rowland circle circumference) progressively changes, and it should not have been taken as constant in [8]. Taking the spectrometer geometry into better account (now for all spectral sections covered), changes the dispersion notably, so that - with reference to the same line of Na-like Xe in the short-wavelength spectrum - the identifications of several other lines change. The consequences are described below.

At the time of the Xe measurements (in 1993), the spectrometer had not yet reached its later higher resolving power (then enabled by a blazed diffraction grating optimized for observation in higher diffraction orders). In principle, the spectra could

be remeasured nowadays with a somewhat better resolution while using the same basic instrument, or with a flat-field spectrograph and a CCD camera, as employed at the Livermore electron beam ion traps [10]. Measurements at other ion beam energies could be used to enhance other charge states. However, priorities at GSI have shifted; the spectrometer has been passed on to another laboratory, and the beam-foil measurement set-up has been dismantled. The same spectral range and charge states can be reached in laser-produced plasmas [34] and in electron beam ion traps [10]. Both of these techniques have different conditions (high vs. low density) and therefore the spectra often look rather different. The beam-foil data are peculiar in the sense that the excitation takes place at very high density, whereas the observation is of ions in a low density environment, and the observation is intrinsically time-resolved on the scale of a few picoseconds.

At the given energy of 5.9 MeV/amu, the expected charge state distribution [35] of the foil-excited Xe ion beam was q=47+ (N-like ions) 2%, 46+ (O-like) 6%, 45+ (F-like) 14%, 44+ (Ne-like) 20%, 43+ (Na-like) 22.5%, 42+ (Mg-like) 18%, 41+ (Al-like) 11%, 40+ (Si-like) 4.5%, and 39+ (P-like) 1.2% (other calculations and tabulations may differ by up to one charge state for the mean or the most abundant charge state). Consequently, when using a sufficiently thick exciter foil (of a few hundred μg/cm^2 areal density, which is still absolutely thin), transitions between low-lying levels of these ions were expected to show in about the same pattern of overall intensities as the charge state distribution. This means about equal prominence of lines from Ne to Mg-like Xe ions, F- and Al-like ions at half this amount, and everything else being much weaker. Indeed, the strongest line was identified at the time (to be corrected below) with a transition in Ne-like Xe, and the weakest lines for which a classification was suggested were associated tentatively with Si-like Xe ions.

4. Comparison of calculational results with observations

According to the expected range of charge states expected in the spectra (see above), MR-MP term energies and lifetimes of excited levels were evaluated for each of these ions. The term energies and lifetimes of three representative ions, Ne-, Al-, and Si-like Xe, are displayed in tables 1 , 2, and 3. For these multivalence-electron ions, very few experimental and theoretical studies are available, whereas for Na- and Mg-like ions a literature search shows many more entries.

In table 1 , theoretical excitation energies (term values) of the lowest 36 excited states of Ne-like Xe ion arising from the 2l-11l' (l=0-1, l'=0-3) configurations are compared with available experimental data [37]. The energies were computed by subtracting the total energy of the ground $1s^2 2s^2 2p^6\ {}^1S_0$ state from those of the excited levels. The term energies of 12 excited levels in the Ne-like ion have been evaluated by MBPT [38]. They are also given in table 1 for comparison. For all the experimentally determined level energies, our MR-MP energies agree well with experiment, a majority of them to within the experimental error.

A fair number of other calculations and semiempirical analyses are available for ions along isoelectronic sequences. These are, for example, for the Ne sequence [38, 39, 40], for Na-like ions [42, 43, 44], for the Mg sequence [45, 46, 47, 48, 49, 50, 51, 52], for Al-like ions [53, 54, 55], and for the Si sequence [56, 57, 58, 59, 60, 61]. With the exception of the Na sequence (of the sequences discussed here), in which experimental tests up to U^{81+} [62] have confirmed the high accuracy of the latest calculations, most isoelectronic sequence calculations are not extremely accurate - aiming for accuracy usually puts high demands on computing power. This is in a way orthogonal to the approach chosen here, the calculation of accurate values for many ions of a given elemental species. Because of the different intentions, we refrain from direct comparisons with the results of other calculations, with the exception of a few examples for which experimental data are available as well (see below).

4.1. Comparison with Xe beam-foil spectra

The beam-foil spectra [8] mostly cover three spectral sections within the wavelength range from 50 to 150 Å. The spectra have been recorded at various foil displacements (up to 28 positions) from the line of sight of the spectrometer, corresponding to observations in a range of delays after excitation. In the short-wavelength parts (50 to 100 Å), results for decays with level lifetimes longer than 2 ps are listed in table 4; in the longer-wavelength part (100 to 150 Å), the typical level lifetimes are also longer, and we have listed decays with characteristic lifetimes longer than 15 ps in table 5. Of the thousands of calculated lines that fall into the range 50-150 Å, we have listed only the strongest E1 lines expected. The observed spectra show much fewer lines; considering the predicted line spacings and the experimental spectral resolution, it is obvious that many of the observed lines must represent line blends.

In order to facilitate the visual comparison of calculated atomic data with observations, we have synthesized spectra on the basis of our calculations. For this aim, line intensities were estimated from transition probabilities and corrected for branch fractions; for the matching of delayed spectra, the atomic decays were followed over a corresponding time interval. For the superposition of spectra from ions in different charge states, the charge state fractions were modified somewhat to improve the visual agreement of predicted and observed spectra; the *ab initio* calculational results for the wavelengths were not altered. No explicit attempt was made to set up a model of initial level populations and cascade repopulation from high-lying levels. Especially with the non-selective ion-foil interaction, high-lying and even multiply excited levels may be populated, and cascade tails play a significant role in the decay curve analysis of few-electron ions. Collisional-radiative models (like those based on the HULLAC [63, 64] or the FAC code [65] specialize in such multilevel population dynamics, but they do not necessarily reach our wavelength accuracy. Therefore the relative line intensities in our synthetic spectra ought to be taken with a grain of salt.

In earlier experimental studies, line identifications have often been guided by

Multi-Configuration Hartree-Fock (MCHF) or Multi-Configuration Dirac-Fock (MCDF) calculations, as was the case in the 1995 study of the beam-foil spectra [8]. Controversy surrounding line identifications almost always stems from the use of MCDF self-consistent field (SCF) approximations in guiding the experimental line identifications, because MCDF fails to accurately account for correlation corrections, and thus, is not accurate enough to uniquely identify spectral lines. Typically the MCDF wavelengths deviate from experiment by as much as 2 Å, rendering the identification of lines in a line-rich spectrum only tentative. It was noted in [8] that one of the calculations for Mg-like ions had predicted the intercombination transition wavelength almost perfectly, whereas the resonance line wavelength was badly off the mark. Such inconsistencies aggravate at higher Z, and are therefore even more pronounced for Au (as will be discussed elsewhere).

Figures 1 and 2 show new lineouts of the beam-foil spectra first presented in [8]. Figure 3 also shows data from that experiment, but is constructed from a different set of observations that had higher spectral resolution (but fewer foil positions which would be needed for lifetime studies). The three figures also contain synthetic spectra of the same spectral ranges, simulated for an appropriate delay time after excitation. The lines marked in figures 1 and 2 are identified in table 4. Figure 3 compares a synthetic spectrum based on nineteen theoretical E1 lines (numbered 1-19 in table 5) with the experimental beam foil spectrum in the 110-150 Å range.

MCDF calculations [53, 56] predict that Al-like ion $3s^2 3p\ ^2P^o_{3/2}$ - $3s3p^2\ ^4P_{5/2}$ and Si-like ion $3s^2 3p^2\ ^3P_2$ - $3s3p^3\ ^5S^o_2$ lines are blended at 128.95-128.96 Å. Therefore, Träbert et al. [8] earlier identified the line at 127.9±1.0 Å as a candidate for the Si-like ion $3s^2 3p^2\ ^3P_2$ - $3s3p^3\ ^5S^o_2$ line and the 130.4 Å line as the blend of Mg-like and Al-like lines (labeled J and K in Ref. [8]). The results of our MR-MP calculations, however, suggest that their line J results from the decay of lowest even-parity J=5 level in the Si-like ion to the lowest odd-parity J=4 level, and not from the $^3P_2$ - $^5S^o_2$ transition. The new assignment refers to a transition not assigned (to our knowledge) in any other Si-like ion; hence there is no expertise and isoelectronic comparison to help judge the validity of the assignment, beyond our calculation and the supporting argument that in beam-foil spectra the levels with the highest J-values often are amply populated, and their decay chains unbranched. However, such particularly long-lived levels far above the ground configuration do occur in quite a number of isoelectronic sequences (for an early discussion, see [66]). They contribute to extended cascade tails in beam-foil lifetime measurements, and they may be of importance in the diagnostics of plasma spectra where they influence the temporal development of discharges by providing highly excited population traps with level lifetimes that differ from most of the neighbouring levels by several orders of magnitude. Their longevity may also provide stepping stones for collisional ionization well below the ionization potential of a given ion, and thus they influence the charge state balance.

Within the experimental uncertainty, the strong lines of the Na- and Mg-like ions were seen in the beam-foil spectra at positions that agreed with preceding measurements on stationary light sources. (A typesetting error occurred in table 1 of ref. [8]: a line

(actually a line blend) at 130.4 Å (old calibration)(see figure 3) was wrongly listed with a wavelength of 134 Å). The observed positions of the transitions in Na-like ions at 123.9±0.5 Å, Mg-like lions at 63.2±0.5 Å and at 130.4±0.5 Å, and of the Al-like ion 122.5±0.5 Å and 147.0±1.0 Å lines agree with the MR-MP prediction within the experimental error. However, the previous identification of the 122.5±0.5 Å line with the $^2P^o_{3/2}$ - $^4P_{1/2}$ transition in the Al-like ion ought to read $^2P^o_{1/2}$ - $^4P_{1/2}$. The predicted Si-like ion $^3P_1$ - $^5S^o_2$ line at 121.604 Å is blended with the Al-like ion line $^2P^o_{1/2}$ - $^4P_{1/2}$ at 122.265 Å. The predicted Si-like ion $^3P_2$ - $^5S^o_2$ line at 129.683 Å is blended with other lines at 130 Å.

It would have been good to observe the two decay branches of the $3s3p^3$ $^5S^o_2$ level; guided by a survey calculation [56], tentative candidate lines for the two transitions have been suggested among the weak lines of the beam-foil spectra [8]. Bengtsson *et al.* [58] declared this suggestion to be grossly wrong, based on their isoelectronic studies that, however, deviated notibly from the well-established trend at lower nuclear charges [54]. When this was pointed out [59], Ishikawa & Vilkas [60] performed new calculations which indicated that probably everybody had been not quite right on these transitions in Si-like Xe (and Au [8, 9]) so far, although only one of the studies mentioned had results that are incompatible with a smooth isoelectronic trend. Another later calculation [61] has wavelength results nearby. The details cannot be sorted out without high-resolution spectra of several ions (isoelectronic trends) in a light source that is running under optimized conditions.

The long-wavelength section of the experimental beam-foil data (mostly featuring 3s - $3p_{1/2}$ transitions; figure 3, table 5) was basically correctly displayed in [8]. The middle section, with the $3p_{3/2}$ - $3d_{5/2}$ transition in Na-like Xe (84.93 Å) as an anchor, required a slight rescaling of the dispersion; it now shows a striking likeliness to the synthetic spectrum (see figure 2) which in turn lends credability to the calculated values and to the thus available identifications of the weak lines in this range (table 4).

The short-wavelength section of the beam-foil spectra required a massive correction to the assumed spectral dispersion. With the wavelength anchor unchanged (the $3p_{1/2}$ - $3d_{3/2}$ transition in Na-like Xe (58.285 Å)), the expected position of the resonance transition $3s^2$ $^1S_0$ - 3s3p $^1P^o_1$ (62.917 Å) is a different line than assumed before. The strongest line of the spectrum, near 66.5 Å, which seemed somewhat mysterious before and then was found to coincide with prediction for a line in Ne-like Xe (see [8]) now turns out to comprise several lines that may be expected to be strong, among them the $3s_{1/2}$ - $3p_{3/2}$ transition in the Na-like Xe ion (66.631 Å). (The line in the Ne-like ion is still present, as part of a cluster of weak lines, calculated at 68.733 Å.) The aforementioned transition in the Na-like ion on its own cannot explain the high overall intensity of the line (although cascade repopulation would easily boost the line intensity beyond the result of our calculations); an important blending partner is the 3s3p $^1P^o_1$ - $3p^2$ $^1D_2$ transition in the Mg-like ion (66.102 Å), which also carries massive cascade repopulation along a chain of yrast levels, that is, of high n, maximum l levels. In low-Z ions, the $3p^2$ $^1D_2$ level lifetime is about four to five times as long as the 3s3p $^1P^o_1$ level lifetime.

In higher-Z ions, however, a decay channel of the $3p^2\ {}^1D_2$ level to the $3s3p\ {}^1P^o_{1,2}$ levels opens up and progressively shortens the $^1D_2$ level lifetime (see discussion in [67, 68, 69]). For Mg-like Xe, the expected lifetime ratio is only about a factor of two, from an about equal branching of the $^1D_2$ level decays without and with spin change.

4.2. Comment on decay curves and lifetimes

One of the unique advantages of the beam-foil light source lies in the fact that it inherently provides time resolution and thus can be used to determine atomic level lifetimes in the ps- to ns-range. This property was the main point of refs. [7, 8]. At the time it was noted that several lines consisted of line blends, representing the decays of levels with not very different lifetimes (similar electronic states in ions that differ by one or a few units of charge). The new calculations indicate that even more decays may have contributed. Owing to the fact that high-lying levels usually are less populated in the excitation process than are low-lying levels, one might argue that the added lines are not expected to have much effect on the apparent lifetimes, and that therefore the previously determined level lifetimes and the experimental error bars do not need to be changed, although the associated level identifications may have been changed in one case or the other. However, the actual situation is more complex.

For example, there are four major 3s - 3p - 3d transitions in the Na-like Xe ion, and previous beam-foil work [7] found them in a pattern of decay curves and extracted lifetimes that was compatible with expectation, although we now know that one of the four lines was misidentified. Similarly, the resonance line in the Mg-like ion was misidentified, but the measured lifetime is in reasonable accord with expectation. The reason for the overall agreement of experiment and calculation lies in the 'type of transition'. The lines in the spectra are grouped by 'type': in Xe, the $3s_{1/2}$ - $3p_{1/2}$ lines have about twice the wavelength of the $3s_{1/2}$ - $3p_{3/2}$ lines; within each 'type', the wavelength (and thus lifetime) differences are small, because the screening differences in Na-, Mg-, and Al-like ions are small, while the oscillator and line strength values are practically the same. Where the spin changes (intercombination transitions), as in the $3s_{1/2}$ - $3p_{1/2}$ transitions of Mg- and Al-like ions, the predicted lifetimes differ by only some 10% - which is quite compatible with the experimental uncertainty. In table 6 we present the previously reported lifetime measurement results in combination with the updated line identifications.

The Mg-like ion line $^1S_0$ - $^3P^o_1$ at 129.95 Å, the Al-like ion line at 130.32 Å, and the Si-like ion line at 129.68 Å are blended. The theoretical MR-MP lifetime value of 160.5 ps for the Mg $^3P^o_1$ level is in good agreement with the MBPT lifetime of 163 ps. In fact, all three of these theoretical lifetimes are in good agreement with the experimental lifetime of 170±30 ps within the experimental uncertainty.

While in some cases the lifetime data can be associated with one dominant contribution to the effective decay curve obtained from a spectral feature, there are other features that consist of too many blended components to ascribe the result of

multiexponential fits to just one level. The measurements agree with expectation in all cases at least in the sense that in the short-wavelength spectral section the typical lifetimes of interest are near 10 ps, and about 100 to 200 ps in the long-wavelength spectra. However, in order to obtain more level-specific lifetime numbers from experiment, measurements with higher spectral resolution are required. The same requirement would hold to find out about the relative importance of various calculated contributions to a given spectral feature.

4.3. Comparison with recent Xe spectra from the Livermore electron beam ion trap

For need of signal, grating spectrometers often operate with much wider slits than would be possible at the diffraction limit. Under such conditions, the line width is dominated by the instrumental line width and is largely independent of wavelength. This implies that at short wavelengths the resolving power $\lambda/\Delta\lambda$ suffers. This is evident in the beam-foil spectra that we show. Higher resolving power would be available, if the Doppler broadening was reduced (for example, by using a stationary light source instead of the fast ion beam), or a grating with a larger Rowland circle radius or of higher groove density. As it happens, there are data available from an electron beam ion trap (Livermore SuperEBIT, a stationary light source) that have been obtained with a grating of similar Rowland circle size (diameter 5 m) and a groove density of 1200 ℓ/mm (four times higher than in the GSI work) [10]. These spectra include the range from 50 to 70 Å(figure 4, table 7). The SuperEBIT spectra cover the other ranges of the beam-foil data set, too. For example, they show the strong lines of figure 4 in second and third diffraction order, but the first diffraction order lines near 130 Å are very weak in those spectra, too weak to merit analysis in the present context.

The SuperEBIT spectra in the 70-Å range are not calibrated to high precision, because the calibration emphasis was on a different range within the operating range of the spectrometer. The spectrum shown in figure 4 is, in fact, from the edge of the working range with a given grating adjustment, and thus the lines of present interest are covered only by an extrapolation of the calibration from the nearest reference points. The agreement of calculated wavelengths and observed spectral features is typically better than 0.05 Å, which is also the estimated calibration uncertainty.

The relative line intensities in the SuperEBIT spectrum are drastically different from those of the beam-foil spectra. Excitation in an electron beam ion trap is (almost) from the true ground state only - this is typical for a low density light source in which there is sufficient time between excitations so that excited levels can decay radiatively before the next collisional excitation takes place. In the high-density environment inside an exciter foil (or in a laser-produced plasma), the collision frequency is so much higher that practically all levels can be reached. The beam-foil spectra are richer (more crowded). This is an advantage as to the avoidance of line blends, of which so many afflict the aforementioned beam-foil spectra. However, our calculations indicate that the strong line of Na-like Xe in the SuperEBIT spectrum, which may be considered

as a wavelength anchor, may be suffering from a blend with a line from the P-like Xe ion, within its rather narrow line width. Even higher spectral resolution will be needed for unambiguous spectral analysis and high-accuracy wavelength determinations. Table 7 identifies the prominent features of the SuperEBIT spectrum according to our calculations and to ref. [10].

5. Conclusion

In the present work we discuss how a series of calculations by a given technique fares on a range of ions of the same element, how spectral simulations can help in revealing assignment errors, and we reanalyze the earlier beam-foil data. In addition, we compare some of the synthetic spectra and the beam-foil data with observations from a light source of very different properties, the electron beam ion trap. Twelve years ago, it was difficult to find out, which strong line might be originating from which transition in which ion. With the new calculations, there are often several reasonable identifications within the measured line profile, and weak lines that have been neglected before can now be identified. Evidently, computations have remarkably improved. They clearly supersede some earlier theoretical work that had served as guidance for the spectral analysis of data beyond the range of nuclear charge Z for which a fairly consolidated body of atomic data existed at the time. The present calculations are the first that treat all Xe ion species of present interest on a comparable level of detail, and the wavelength results are good enough to enable instant line identifications with transitions in a fair range of ion charge states.

The new calculations enhance and expand the interpretation of the available beam-foil spectra. They also predict the spectral features to be expected in adjacent spectral ranges. This is a most valuable practical tool for spectral exploration. A comparison with EUV spectra from an electron beam ion trap (which offers higher spectral resolution than the beam-foil technique, but has no comparable time resolution) reveals excellent agreement with the spectral structure seen in such an experiment. The EBIT spectra represent much more selective excitation features than does the ion-foil interaction, but the higher experimental precison obtainable, in combination with accurate calculations, seems to be superior to most spectral analyses based on the beam-foil technique alone.

The identification of almost all features in the line rich EUV spectra of, both, foil-excited Xe ion beams and the Xe ions stored in an electron beam ion trap would have been almost impossible without detailed guidance by calculation. The present calculations appear to be not merely useful in this context; they are superior in wavelength accuracy to measurements that have not been trained to yield utmost wavelength accuracy (which likely can be achieved only under very favourable circumstances), and they actually compete with precise experiments. To put these claims into numbers: The deviation between our calculational results and experimentally established wavelengths for prominent lines in Na- and Mg-like Xe [34, 71] is of the order of 0.05 Å. We expect similar uncertainties for the other isoelectronic sequences,

once experiment provides hard data. In contrast, the deviation of other calculations from our results (and thus most likely also from the proper experimental values) is ten to fourty times larger. Although the moderate spectral resolution of the beam-foil data is insufficient to resolve various line blends, the data rule out a number of earlier calculational results while being fully compatible with our calculations.

Acknowledgments

This research is supported in part by the U.S-Israel Binational Science Foundation. ET acknowledges travel support from the German Research Association (DFG). Part of this work has been performed at LLNL under the auspices of the USDoE under contract No. W-7405-ENG-48.

References

[1] In the World Wide Web at http://Physics.nist.gov/PhysRefData/contents.html
[2] Bastin T, Biémont E, Dumont P-D, Garnir H-P, Krenzer M J and Bukow H 1997 *J. Opt. Soc. Am.* **14** 1319
[3] Bastin T, Biémont E, Dumont P-D, Garnir H-P, Krenzer M J, Bukow H and Kramida A E 1997 *Phys. Scr.* **55** 654
[4] Kramida A E, Bastin T, Biémont E, Dumont P-D, Garnir H-P 1999 Eur. Phys. J. D **7** 525
[5] Kramida A E, Bastin T, Biémont E, Dumont P-D and Garnir H-P 1999 Eur. Phys. J. D **7** 547
[6] Kramida A E, Bastin T, Biémont E, Dumont P-D, Garnir H-P 1999 *J. Opt. Soc. Am.* **16** 1966
[7] Träbert E, Doerfert J, Granzow J, Büttner R, Staude U, Schartner K-H, Rymuza P, Mokler P H, Engström L and Hutton R 1994 *Phys. Lett.* A **188** 355
[8] Träbert E, Doerfert J, Granzow J, Büttner R, Staude U, Schartner K-H, Rymuza P, Engström L and Hutton R 1995 *Z. Phys.* D **32** 295
[9] Träbert E, Staude U, Bosselmann P, Schartner K-H, Mokler P H and Tordoir X 1998 Eur. Phys. J. D **2** 117
[10] Träbert E, Beiersdorfer P, Lepson J K, Chen H 2003 *Phys. Rev.* A **68** 042501
[11] Dietrich D D, Chandler G A, Fortner R J, Hailey C J, Stewart R E 1985 *Phys. Rev. Lett.* **54** 1008
[12] Beiersdorfer P, von Goeler S, Bitter M, Hinnov E, Bell K, Bernabei S, Felt J, Hill K W, Hulse R, Stevens J, Suckewer S, Timberlake J, Wouters A, Chen M H, Scofield J H, Dietrich D D, Gerassimenko M, Silver E, Walling R S and Hagelstein P 1988 *Phys. Rev.* A **37** 4153
[13] Aglitskii E V, Ivanova E P, Panin S A, Safronova U I, Ulityn S I, Vainshtein L A and Wyart J-F 1989 *Phys. Scr.* **40** 601
[14] Churilov S S, Joshi Y N, Reader J and Kildiyarova R R 2004 *Phys. Scr.* **70** 126
[15] Tanuma H, Ohashi H, Shibuya E, Kobayashi N, Okuno T, Fujioka S, Nishimura H and Nishihara K 2005 *Nucl. Instrum. Methods* B **235** 331
[16] Biedermann C, Radtke R, Fußmann G, Schwob J L and Mandelbaum P 2005 *Nucl. Instrum. Methods* B **235** 126
[17] Sucher J 1980 *Phys. Rev.* A **22** 348
[18] Mittleman M H 1981 *Phys. Rev.* A **24** 1167
[19] Vilkas M J, Ishikawa Y and Koc K 1998 *Phys. Rev.* E **58** 5096
[20] Savukov I M and Johnson W R 2002 *Phys. Rev.* A **65** 042053
[21] Møller C and Plesset M S 1934 *Phys. Rev.* **46** 618
[22] Vilkas M J and Ishikawa Y 2003 *Phys. Rev.* A **68** 012503
[23] Vilkas M J and Ishikawa Y 2004 *Phys. Rev.* A **69** 062503

[24] Ishikawa Y, Quiney H M and Malli G L 1991 *Phys. Rev.* A **43** 3270
[25] Indelicato P, Gorceix O and Desclaux J P 1987 *J. Phys. B: At. Mol. Phys.* **20** 651
[26] Kim Y-K 1990 in *Atomic Processes in Plasmas*, AIP Conf. Proc. No. 206 p. 19
[27] Mohr P J 1992 *Phys. Rev.* A **46** 4421
[28] Büttner R, Kraus B, Schartner K-H, Folkmann F, Mokler P H and Möller G 1992 *Z. Phys.* D **22** 693
[29] Staude U, Bosselmann Ph, Büttner R, Horn D, Schartner K-H, Folkmann F, Livingston A E, Ludziejewski Th and Mokler P H 1998 *Phys. Rev.* A **58** 3516
[30] Bosselmann Ph, Staude U, Horn D, Schartner K-H, Folkmann F, Livingston A E and Mokler P H 1999 *Phys. Rev.* A **59** 1874
[31] Feili D, Bosselmann P, Schartner K-H, Folkmann F, Livingston A E, Träbert E, Ma X and Mokler P H 2000 *Phys. Rev.* A **62** 022501
[32] Feili D, Zimmermann B, Neacsu C, Bosselmann P, Schartner K-H, Folkmann F, Livingston A E, Träbert E and Mokler P H 2005 *Phys. Scr.* **71** 48
[33] Ekberg J O, Feldman U, Seely J F and Brown C M 1989 *Phys. Scr.* **40** 643
[34] Ekberg J O, Feldman U, Seely J F, Brown C M, MacGowan B J, Kania D R and C. J. Keane 1991 *Phys. Scr.* **43** 19
[35] Shima K, Kuno N, Yamanouchi M and Tawara H 1992 *At. Data Nucl. Data Tables* **51**, 173
[36] LIvingston A E, Büttner R, Zacarias A S, Kraus B, Schartner K-H, Folkmann F and Mokler P H 1997 *J. Opt. Soc. Am.* **14** 522
[37] Beiersdorfer P, von Goeler S, Bitter M, Hinnov E, Bell R, Bernabei S, Felt J, Hill K W, Hulse R, Stevens J, Suckewer S, Timberlake J, Wouters A, Chen M H, Scofield J H, Dietrich D D, Gerassimenko M, Silver E, Walling R S, Hagelstein P L 1988 *Phys. Rev.* A **37** 4153
[38] Safronova U I, Safronova M S, Bruch R 1994 *Phys. Scr.* **49** 446
[39] Cogordan J A, Lunell S 1986 *Phys. Scr.* **33** 406
[40] Ivanova E P and Gulov A V 1991 *At. Data Nucl. Data Tables* **49** 1
[41] Theodosiou C E and Curtis L J 1988 *Phys. Rev.* A **38** 4435
[42] Johnson W R, Blundell S A and Sapirstein J 1988 *Phys. Rev.* A **38** 2699
[43] Kim Y-K, Baik D H, Indelicato P and Desclaux J P 1991 *Phys. Rev.* A **44** 148
[44] Blundell S A 1993 *Phys. Rev.* A **47** 1790
[45] Cheng K T and Johnson W R 1977 *Phys. Rev.* A **16** 263
[46] Ivanov L N and Ivanova E P 1979 *At. Data Nucl. Data Tables* **24** 95
[47] Curtis L J and Ramanujam P S 1983 *J. Opt. Soc. Am.* **73** 979
[48] Ivanova E P, Ivanov L N and Tsirekidze M A 1986 *At. Data Nucl. Data Tables* **35** 419
[49] Curtis L J 1991 *Phys. Scr.* **43** 137
[50] Marques J P, Parente F and Indelicato P 1993 *At. Data Nucl. Data Tab.* **55** 157
[51] Safronova U I, Johnson W R and Berry H G 2000 *Phys. Rev.* A **61** 052503
[52] Zou Y and Froese Fischer C 2001 *J. Phys. B: At. Mol. Opt. Phys.* **34** 915
[53] Huang K-N 1986 *At. Data Nucl. Data Tables* **34** 1
[54] Jupén C and Curtis L J 1996 *Phys. Scr.* 53 312
[55] Safronova U I, Namba C, Albritton J R, Johnson W R and Safronova M S 2002 *Phys. Rev.* A **65** 022507
[56] Huang K-N 1985 *At. Data Nucl. Data Tables* **32** 503
[57] Jupén C, Martinson I and Denne-Hinnov B 1991 *Phys. Scr.* 44 562
[58] Bengtsson P, Ando K, Kambara T, Awaya Y and Hutton R 1997 *Phys. Scr.* T **73** 81
[59] Träbert E 1999 *Phys. Scr.* **59** 443
[60] Ishikawa Y and Vilkas M J 2002 *Phys. Scr.* **65** 219
[61] Huang M, Andersson M, Brage T, Hutton R, Jönsson P, Chongyang C and Zou Y 2005 *J. Phys. B: At. Mol. Opt. Phys.* **38** 503
[62] Beiersdorfer P, Träbert E, Chen H, Chen M-H, May M J and Osterheld A L 2003 *Phys. Rev.* A **67** 052103

[63] Bar-Shalom A, Klapisch M and Oreg J 1988 *Phys. Rev.* A **38** 1773
[64] Bar-Shalom A, Klapisch M and Oreg J 2001 *J. Quant. Spectrosc. Radiat. Transfer* **71** 169
[65] Gu M F 2003 *Astrophys. J.* **582** 1241
[66] Träbert E 1981 *Phys. Scr.* **23** 253
[67] Froese Fischer C and Godefroid M 1982 *Nucl. Instrum. Methods* B **202** 307
[68] Hutton R, Engström L and Träbert E 1988 *Nucl. Instrum. Methods* B **31** 294
[69] Träbert E, Pinnington EH, Kernahan J A, Doerfert J, Granzow J, Heckmann P H and Hutton R 1996 *J. Phys. B: At. Mol. Phys.* **29** 2647
[70] Safronova U I, Namba C, Murakami I, Johnson W R and Safronova M S 2001 *Phys. Rev.* A **64** 012507
[71] Reader J, Kaufman V, Sugar J, Ekberg J O, Feldman U, Brown C M, Seely J F and Rowan W L 1987 *J. Opt. Soc. Am.* B **4** 1821

This work was performed under the auspices of the U. S. Department of Energy by University of California, Lawrence Livermore National Laboratory under contract W-7405-Eng-48.

Tables and table captions

Table 1. Comparison of the MR-MP calculated excitation energies E (eV) and lifetimes τ with experimental and other theoretical results in Ne-like xenon ions.

Level	J	E(MR-MP)	τ (ps)	E(Expt)[a]	E(MCDF)[a]	E(MBPT)[b]	Label
$2s^2 2p_{1/2}^2 p_{3/2}^4$	0	0		0	0	0	0(1)
$2p_{3/2}^{-1} 3s_{1/2}$	2	4210.02		4210.2(2)	4208.88	4209.9	2(1)*
$2p_{3/2}^{-1} 3s_{1/2}$	1	4215.48	0.030	4215.2(2)	4214.44	4215.21	1(1)*
$2p_{3/2}^{-1} 3p_{1/2}$	1	4302.56	55.757				1(1)
$2p_{3/2}^{-1} 3p_{1/2}$	2	4304.97	54.421	4305.3(2)	4304.29	4304.8	2(1)
$2p_{3/2}^{-1} 3p_{3/2}$	3	4390.41	7.072				3(1)
$2p_{3/2}^{-1} 3p_{3/2}$	1	4390.42	7.854				1(2)
$2p_{3/2}^{-1} 3p_{3/2}$	2	4398.68	6.355	4398.8(3)	4397.93	4398.5	2(2)
$2p_{3/2}^{-1} 3p_{3/2}$	0	4433.07	3.761				0(2)
$2p_{3/2}^{-1} 3d_{3/2}$	0	4497.26	7.801				0(1)*
$2p_{3/2}^{-1} 3d_{3/2}$	1	4503.08	0.586			4502.47	1(2)*
$2p_{3/2}^{-1} 3d_{3/2}$	3	4506.55	7.077				3(1)*
$2p_{3/2}^{-1} 3d_{3/2}$	2	4510.75	6.715				2(2)*
$2p_{3/2}^{-1} 3d_{5/2}$	4	4523.26	0.971				4(1)*
$2p_{3/2}^{-1} 3d_{5/2}$	2	4527.39	19.385				2(3)*
$2p_{3/2}^{-1} 3d_{5/2}$	3	4534.26	18.684				3(2)*
$2p_{1/2}^{-1} 3s_{1/2}$	1	4543.69	0.006	4543.5(2)	4542.42	4543.51	1(3)*
$2p_{1/2}^{-1} 3s_{1/2}$	0	4544.26	112.51				0(2)*
$2p_{3/2}^{-1} 3d_{5/2}$	1	4557.76	0.002	4557.8(2)	4557.75	4557.96	1(4)*
$2p_{1/2}^{-1} 3p_{1/2}$	1	4636.26	55.637				1(3)
$2p_{1/2}^{-1} 3p_{1/2}$	0	4666.87	11.070				0(3)
$2p_{1/2}^{-1} 3p_{3/2}$	1	4725.09	6.400				1(4)
$2p_{1/2}^{-1} 3p_{3/2}$	2	4727.89	6.918	4728.4(5)	4726.92	4727.7	2(3)
$2p_{1/2}^{-1} 3d_{3/2}$	2	4839.77	6.952				2(4)*
$2s_{1/2}^{-1} 3s_{1/2}$	1	4854.37	0.466				1(5)
$2p_{1/2}^{-1} 3d_{3/2}$	1	4856.89	0.002	4857.4(2)	4856.20	4856.78	1(5)*
$2p_{1/2}^{-1} 3d_{5/2}$	2	4860.69	18.151				2(5)*
$2p_{1/2}^{-1} 3d_{5/2}$	3	4863.39	19.613				3(3)*
$2s_{1/2}^{-1} 3s_{1/2}$	0	4872.40	0.565				0(4)
$2s_{1/2}^{-1} 3p_{1/2}$	0	4947.12	0.496				0(3)*
$2s_{1/2}^{-1} 3p_{1/2}$	1	4949.10	0.024	4949.2(4)	4951.60	4948.7	1(6)*
$2s_{1/2}^{-1} 3p_{3/2}$	2	5035.54	0.466				2(6)*
$2s_{1/2}^{-1} 3p_{3/2}$	1	5039.68	0.010	5039.9(2)	5042.03	5039.3	1(7)*
$2s_{1/2}^{-1} 3d_{3/2}$	1	5146.70	0.523				1(6)
$2s_{1/2}^{-1} 3d_{3/2}$	2	5149.98	0.491				2(4)
$2s_{1/2}^{-1} 3d_{5/2}$	3	5166.71	0.510				3(2)
$2s_{1/2}^{-1} 3d_{5/2}$	2	5178.39	0.523	5178.8(2)	5181.22	5178.1	2(5)

a [37]. The experimental error is about ± 1200 cm^{-1}. *b* [70].

Table 2. MR-MP calculated term values E and lifetimes τ in Al-like xenon ions. The five-digit number shows the occupation $n_{3s1/2}n_{3p1/2}n_{3p3/2}n_{3d3/2}n_{3d5/2}$ of the relativistic shells of the dominant CSF.

Level		E (cm^{-1})	τ (ps)	Level		E (cm^{-1})	τ (ps)
21000	1/2(1)*	0		10110	3/2(9)*	3483350	2.369
20100	3/2(1)*	665774		10101	7/2(3)*	3498082	5.665
12000	1/2(1)	817897	87.00	10110	5/2(7)*	3525761	1.741
11100	3/2(1)	1343238	795.8	02010	3/2(5)	3528947	11.69
11100	5/2(1)	1433127	202.1	10110	1/2(5)*	3540680	1.752
11100	3/2(2)	1557533	10.96	10101	7/2(4)*	3588466	3.300
11100	1/2(2)	1622936	2.915	10101	1/2(6)*	3650470	3.043
20010	3/2(3)	1916301	2.215	10101	3/2(10)*	3696903	2.312
20001	5/2(2)	1963221	82.22	10101	5/2(8)*	3711355	2.058
10200	5/2(3)	2161052	5.107	02001	5/2(4)	3734715	8.798
10200	1/2(3)	2292721	4.161	01110	5/2(5)	4060131	8.098
10200	3/2(4)	2332373	2.110	01110	3/2(6)	4103755	4.188
02100	3/2(2)*	2391645	9.923	01110	1/2(4)	4119363	3.941
11010	3/2(3)*	2503658	28.36	01110	7/2(1)	4125697	6.648
11010	5/2(1)*	2564648	110.1	01101	7/2(2)	4242272	5.372
11010	1/2(2)*	2705035	2.934	01110	3/2(7)	4258726	2.321
11010	3/2(4)*	2714275	3.030	01110	5/2(6)	4261135	2.469
11001	5/2(2)*	2727239	12.21	01101	9/2(1)	4290977	8.613
11001	7/2(1)*	2776926	20.99	01110	1/2(5)	4291867	2.399
11001	5/2(3)*	2834659	12.14	01101	3/2(8)	4311236	3.674
11001	3/2(5)*	2840974	4.675	01101	5/2(7)	4330335	4.481
01200	5/2(4)*	3057098	5.256	01101	7/2(3)	4393739	5.352
01200	3/2(6)*	3105346	2.307	01101	5/2(8)	4443110	2.856
01200	1/2(3)*	3134007	3.791	10020	3/2(9)	4457748	2.295
10110	3/2(7)*	3254258	3.639	01101	1/2(6)	4476240	4.264
10110	5/2(5)*	3256826	2.930	01101	3/2(10)	4493749	2.840
10110	1/2(4)*	3260609	4.156	10020	5/2(9)	4509194	1.941
10110	7/2(2)*	3273673	4.447	10011	7/2(4)	4601137	2.767
10101	9/2(1)*	3290408		10020	1/2(7)	4610848	1.693
10101	3/2(8)*	3389679	3.923	10011	5/2(10)	4648943	2.320
10101	5/2(6)*	3421967	5.689	10011	9/2(2)	4664203	3.508

Table 3. MR-MP calculated term values E (cm^{-1}) and lifetimes τ in Si-like xenon ions. The five-digit number shows the occupation $n_{3s1/2}n_{3p1/2}n_{3p3/2}n_{3d3/2}n_{3d5/2}$ of the relativistic shells of the dominant CSF.

State		E (cm^{-1})	τ (ps)	State		E (cm^{-1})	τ (ps)
22000	0(1)	0		10300	1(7)*	3047160	1.606
21100	1(1)	595487		11110	2(5)	3085628	11.98
21100	2(1)	646721		11110	0(3)	3120579	44.90
20200	2(2)	1279395		11110	1(3)	3139253	83.22
20200	0(2)	1391729		11110	3(2)	3162322	56.88
12100	2(1)*	1417831	116.9	02200	2(6)	3167256	6.464
12100	1(1)*	1577544	10.38	02200	0(4)	3187421	5.995
21010	2(2)*	1779932	716.2	11110	4(1)	3232268	178.6
11200	2(3)*	1917844	534.1	11101	4(2)	3271090	667.0
21001	3(1)*	1979153	94.41	11110	2(7)	3316976	6.272
21010	1(2)*	1994272	1.648	11110	3(3)	3326987	3.789
21001	2(4)*	2106886	6.011	11110	2(8)	3365895	3.350
11200	3(2)*	2128563	12.39	11110	1(4)	3374676	2.640
11200	0(1)*	2162316	12.98	11101	5(1)	3376651	132.7
11200	1(3)*	2226461	7.412	11101	2(9)	3384409	4.445
11200	2(5)*	2257252	4.170	11101	1(5)	3396680	6.514
11200	1(4)*	2309977	2.222	11110	3(4)	3415005	4.125
20110	2(7)*	2584398	1.610	11101	3(5)	3443613	8.609
20101	2(6)*	2585651	71.82	11110	1(6)	3458254	2.924
20110	3(3)*	2587049	2.596	11101	2(10)	3505362	4.635
20110	1(5)*	2587761	1.947	11101	4(3)	3516521	14.89
20101	4(1)*	2593372		11101	3(6)	3525632	3.745
20110	0(2)*	2599675	2.252	11110	1(7)	3545746	1.582
12010	1(2)	2619663	55.74	11110	0(5)	3557355	2.888
12010	2(3)	2650610	58.67	11101	3(7)	3585626	4.278
20101	3(4)*	2796197	3.839	11101	4(4)	3586432	5.707
20101	1(6)*	2821938	5.558	11101	1(8)	3603678	6.940
12001	3(1)	2825716	18.29	11101	1(9)	3671712	4.404
12001	2(4)	2884305	17.57	11101	3(8)	3681780	2.880
10300	2(8)*	2905186	2.655	11101	0(6)	3702300	2.522

Table 4. Strongest E1 decay lines and transition probabilities A in xenon ion in the wavelength range 50 - 110 Å. The upper levels are selected with lifetimes τ larger than 15 ps to simulate delayed measurements. The Roman numeral labels in the first column refer to the spectral features in figures 1 and 2.

Label	λ (Å)	Upper level	τ (ps)	Lower level	A(s^{-1})	$A^2\tau$	
I	52.155	1/2(4)*	4.156	3/2(1)	2.273(+11)	2.147(+11)	Al-like
	52.184	3/2(3)	2.215	1/2(1)*	4.513(+11)	4.510(+11)	Al-like
	52.258	5/2(5)*	2.930	3/2(1)	1.014(+11)	3.013(+10)	Al-like
	52.328	3/2(7)*	3.639	3/2(1)	2.187(+11)	1.741(+11)	Al-like
II	54.582	5(4)*	2.887	5(1)	2.629(+11)	1.995(+11)	Si-like
	54.834	5/2(5)*	2.930	5/2(1)	2.242(+11)	1.473(+11)	Al-like
	55.180	2(2)	3.960	1(1)*	2.497(+11)	2.470(+11)	Mg-like
III	58.285	3/2(1)	5.785	1/2(1)*	1.659(+11)	1.592(+11)	Na-like
IV	60.924	2(4)*	7.011	1(3)	1.376(+11)	1.328(+11)	Ne-like
	61.465	1/2(3)	4.161	3/2(1)*	2.355(+11)	2.308(+11)	Al-like
	61.509	3(1)*	7.184	2(1)	1.343(+11)	1.295(+11)	Ne-like
	61.617	1/2(2)	2.915	1/2(1)*	3.302(+11)	3.179(+11)	Al-like
	61.833	1(2)*	1.274	1(1)	1.067(+11)	1.449(+10)	Ne-like
V	62.916	1(1)	4.706	0(1)*	1.194(+11)	6.714(+10)	Mg-like
	62.917	1(2)*	3.645	0(1)	2.743(+11)	2.743(+11)	Mg-like
	63.682	0(1)*	7.941	1(1)	1.232(+11)	1.205(+11)	Ne-like
	63.823	0(1)*	12.98	1(1)	7.704(+10)	7.704(+10)	Si-like
	64.059	7/2(1)	6.648	5/2(1)*	1.147(+11)	8.744(+10)	Al-like
	64.204	3/2(2)	10.96	1/2(1)*	8.388(+10)	7.709(+10)	Al-like
	64.707	7/2(3)	8.756	5/2(3)*	1.110(+11)	1.078(+11)	F-like
	64.807	0(3)	44.90	1(1)*	1.789(+10)	1.437(+10)	Si-like
VI	66.102	2(1)	13.08	1(1)*	5.696(+10)	4.245(+10)	Mg-like
	66.631	3/2(1)*	7.363	1/2(1)	1.572(+11)	1.572(+11)	Na-like
	66.877	5/2(3)	5.107	3/2(1)*	1.958(+11)	1.958(+11)	Al-like
VII	75.958	3(1)	11.63	2(1)*	8.597(+10)	8.597(+10)	Mg-like
VIII	78.988	3(1)*	16.53	2(1)	3.153(+10)	1.644(+10)	Mg-like
IX	84.930	5/2(1)	15.34	3/2(1)*	6.520(+10)	6.520(+10)	Na-like
X	87.027	4(2)	7.077	3(3)*	1.022(+11)	7.394(+10)	Mg-like
XI	91.433	2(5)*	18.56	1(4)	4.371(+10)	3.545(+10)	Ne-like
	91.454	3(2)*	19.10	2(2)	4.037(+10)	3.114(+10)	Ne-like
	91.502	3(3)*	20.09	2(3)	4.944(+10)	4.911(+10)	Ne-like
	93.333	4(1)*	21.49	3(1)	4.654(+10)	4.654(+10)	Ne-like

Table 5. Strongest E1 decay lines and transition probabilities A in xenon ion in the wavelength range 110 - 150 Å. The upper levels are selected with lifetimes larger than 15 ps to simulate delayed measurements. The numbers in the first column refer to the lines in figure 3.

No	λ (Å)	Upper level	τ (ps)	Lower level	A(s^{-1})	$A^2\tau$	Sequence
1	110.093	0(2)	14.67	1(1)*	6.815(+10)	6.81(+10)	Mg-like
2	114.853	2(3)	58.67	2(2)*	7.123(+09)	2.977(+09)	Si-like
3	117.396	3(1)*	16.07	3(1)	1.279(+10)	2.703(+09)	Mg-like
4	119.086	1(2)	55.74	2(2)*	9.482(+09)	5.012(+09)	Si-like
5	120.261	9/2(1)*	88.27	7/2(2)	8.145(+09)	5.856(+09)	P-like
6	121.604	2(1)*	116.9	1(1)	4.989(+09)	2.910(+09)	Si-like
7	122.265	1/2(1)	96.63	1/2(1)*	1.149(+10)	1.149(+10)	Al-like
8	123.937	1/2(1)*	42.70	1/2(1)	2.342(+10)	2.342(+10)	Na-like
9	127.668	5(1)	132.7	4(1)*	7.533(+09)	7.533(+09)	Si-like
10	129.683	2(1)*	116.9	2(1)	3.563(+09)	1.485(+09)	Si-like
10	129.953	1(1)*	160.54	0(1)	6.161(+09)	6.161(+09)	Mg-like
11	130.318	5/2(1)	184.99	3/2(1)*	4.949(+09)	4.949(+09)	Al-like
12	132.262	2(2)*	34.15	1(2)	1.011(+10)	3.548(+09)	Mg-like
13	133.945	1(3)	56.97	1(3)*	9.865(+09)	5.544(+09)	Ne-like
13	133.991	1(1)	57.86	2(1)*	1.555(+10)	1.399(+10)	Ne-like
14	134.768	1(3)	56.97	0(2)*	5.812(+09)	1.924(+09)	Ne-like
15	138.554	2(1)	56.28	1(1)*	8.145(+09)	3.733(+09)	Ne-like
16	139.999	1/2(4)*	76.05	3/2(4)	5.286(+09)	2.125(+09)	F-like
17	141.375	5/2(1)*	76.12	5/2(1)	7.384(+09)	4.151(+09)	F-like
18	145.606	3/2(2)*	29.86	5/2(1)	1.088(+10)	3.537(+09)	F-like
19	147.554	4(2)	667.0	4(1)*	1.043(+09)	7.252(+08)	Si-like
19	147.609	3/2(1)	795.8	3/2(1)*	7.179(+09)	4.101(+08)	Al-like

Table 6. Beam-foil lifetimes [7, 8] and updated Xe line identifications. The elemental symbols Ne, Na, Mg, Al and Si denote the isoelectronic sequences. Transitions are given in LS-coupling where recognizable; otherwise the standard labeling convention (J-value, parity, running index from lowest level of given J) is referred to; this and the wavelength value enable identification with entries in tables 4 and 5. Wavelength and lifetime values marked with an asterisk (*) are from this work.

Wavelength λ (nm) Observed	λ (nm) Reference	Sequence and transition	Lifetime τ (ps) Observed	τ (ps) Predicted
58.2	58.229 [71]	Na 3p $^2P^o_{1/2}$ - 3d $^2D_{3/2}$	6±1.2	5.62 [41, 43]
	58.285 *			5.79 *
61.3±0.3			5±1.5	
	60.924 *	Ne 4th odd J=2 level		7.01 *
	61.465 *	Al 3rd even J=1/2 level		4.16 *
	61.509 *	Ne 1st odd J=3 level		7.18 *
	61.617 *	Al 2nd even J=1/2 level		2.92 *
	61.833 *	Ne 2nd odd J=1 level		1.27 *
63.8±0.5	62.895 [34]	Mg 3s^2 $^1S_0$ - 3s3p $^1P^o_1$	6.8±0.6	3.54 [45]
	72.14 [46]			3.21 [49]
	62.916 *			4.71 *
	63.682 *	Ne 2p^5 3s $^3P_1$ - 2p^5 3p $^3P_0$		7.94 *
	63.823 *	Si 3s^2 3p^2 $^3P_1$ - 3s 3p^3 $^3P_0$		13.0 *
	64.059 *	Al 1st odd J=7/2 level		6.65 *
	64.204 *	Al 3s^2 3p $^2P^o_{1/2}$ - 3s 3p^2 $^2D_{3/2}$		11.0 *
	66.102 *	Mg 3s3p $^3P^o_1$ - 3p^2 $^1D_2$		13.1 *
66.5	66.541 [71]	Na 3s $^2S_{1/2}$ - 3p $^2P^o_{3/2}$	14±1.5	6.27 [41, 43]
	66.631 *			7.36
	66.877 *	Al 3rd even J=5/2 level		5.11 *
84.8	84.814 [71]	Na 3p $^2P^o_{3/2}$ - 3d $^2D_{5/2}$	14±4	14.9 [41]
				15 [43]
	84.930 *			15.3 *
120±0.1				
	120.65 [56]	Si 3s^{2}3p^2 $^3P_1$ - 3s3p^3 $^5S^o_2$		111 [56]
	121.604 *			117 *
122.4±0.2	121.15 [53]	Al 3s^{2}3p $^2P^o_{1/2}$ - 3s3p^2 $^4P_{1/2}$		83 [53]
	122.265 *			96.6 *
123.9	123.897 [71]	Na 3s $^2S_{1/2}$ - 3p $^2P^o_{1/2}$	42±3	42 [41, 43]
	123.937 *			42.7 *
127.9±0.1	127.668 *	Si 1st even J=5 level		133 *
	128.95 [56]	Si 3s^{2}3p^2 $^3P_2$ - 3s3p^3 $^5S^o_2$		111 [56]
	129.683 *	Si		117 *
	128.96 [53]	Al 3s^{2}3p $^2P^o_{3/2}$ - 3s3p^2 $^4P_{5/2}$		191 [53]
	130.318 *			185 *
130.0±0.1	129.92 [34]	Mg 3s^2 $^1S_0$ - 3s3p $^3P^o_1$	170±30	158 [45]
	129.92 [46]			153 [49]
	129.953 *	Mg		161
133.3±0.3				
	146.3 [53]	Al 3s^{2}3p $^2P^o_{3/2}$ - 3s3p^2 $^4P_{3/2}$		762 [53]
	147.609 *			796 *

Table 7. EBIT spectrum of xenon ions. The letter labels refer to spectral features in figure 4. Experimental wavelength uncertainties are about 0.05 Å.

Label	λ_{expt}	λ_{theor}	Upper level	τ (ps)	Lower level	A (s^{-1})	$A^2\tau$	
A	66.60	66.631	3/2(1)*	7.363	1/2(1)	1.572(+11)	1.572(+11)	Na-like
B	63.35	63.390	1(1)*	10.38	0(1)	7.87(+10)	6.43(+10)	Si-like
C	62.88	62.917	1(2)*	3.645	0(1)	2.743(+11)	2.743(+11)	Mg-like
D	61.58	61.617	1/2(2)	2.915	1/2(1)*	3.302(+11)	3.179(+11)	Al-like
E	52.07	52.184	3/2(3)	2.215	1/2(1)*	4.513(+11)	4.510(+11)	Al-like
F	50.03	50.144	1(2)*	1.648	0(1)	6.03(+11)	5.99(+11)	Si-like

Figure captions

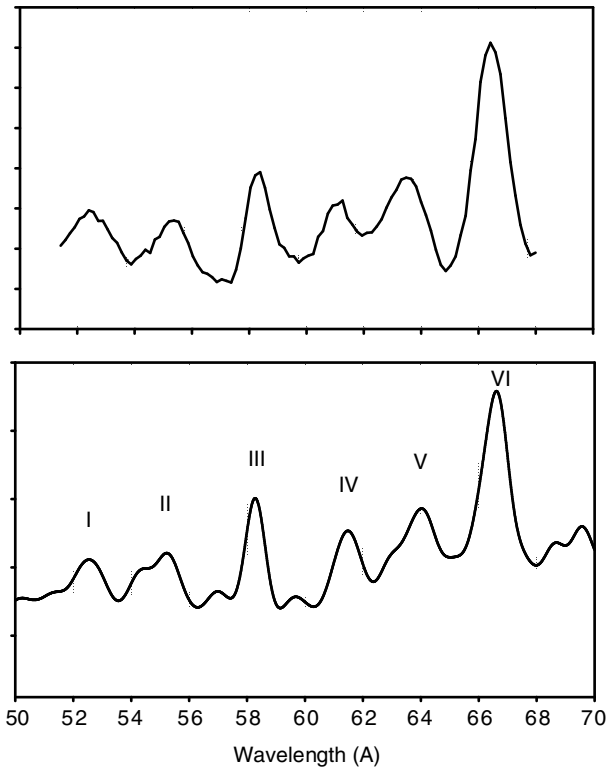

Figure 1. Experimental (top) and synthetic (bottom) spectra of xenon ions in the wavelength range 50-70 Å. Three samples of Xe spectra after beam-foil excitation of 5.9 MeV/amu ^{129}Xe ion beams (replotted beam-foil data of [7, 8]) and synthetic spectra of the same spectral sections as obtained from our present calculations. Na, Mg, and Al denote the isoelectronic sequences of the corresponding Xe lines. Approximate charge state fractions: F-like ions 0.05, Ne-like 0.10, Na-like 0.55, Mg-like 0.20, Al-like 0.12, Si-like 0.05, and P-like 0.01. Branching was accounted for. Simulated for a delay time of 10 ps.

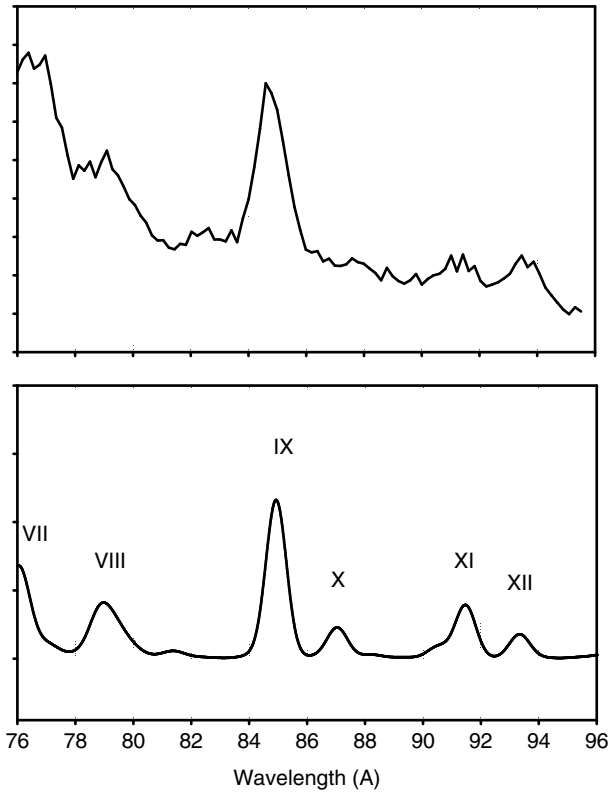

Figure 2. Experimental (top) and synthetic (bottom) spectra of xenon ions in the wavelength range 76-96 Å (replotted beam-foil data of [7, 8]). Approximate charge state fractions: F-like ions 0.05, Ne-like 0.10, Na-like 0.55, Mg-like 0.20, Al-like 0.12, Si-like 0.05, and P-like 0.01. Branching was accounted for. Simulated for a delay time of 10 ps.

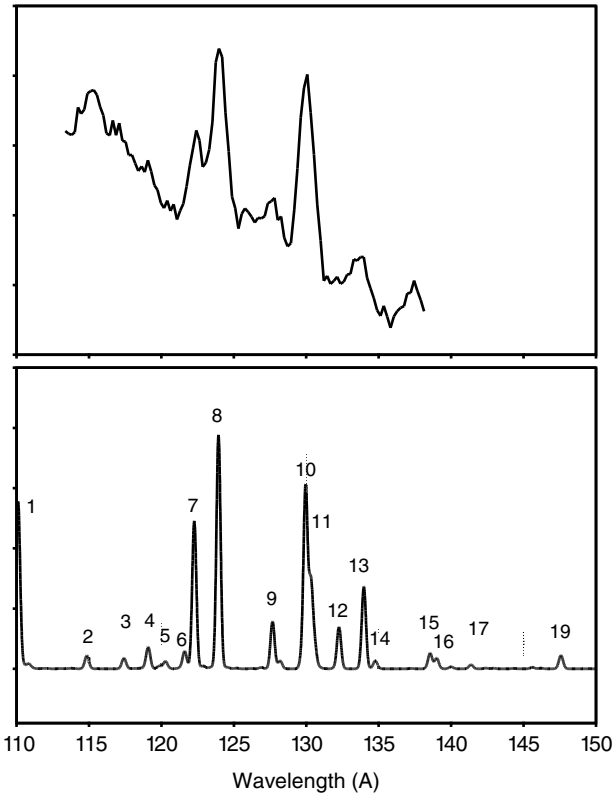

Figure 3. Experimental (top) and synthetic (bottom) spectra of xenon ions in the wavelength range 110-150 Å (beam-foil data of [7, 8]). Approximate charge state fractions: F-like ions 0.02, Ne-like 0.13, Na-like 0.32, Mg-like 0.35, Al-like 0.18, Si-like 0.08, and P-like 0.02. Branching was accounted for. Simulated for a delay time of 40 ps.

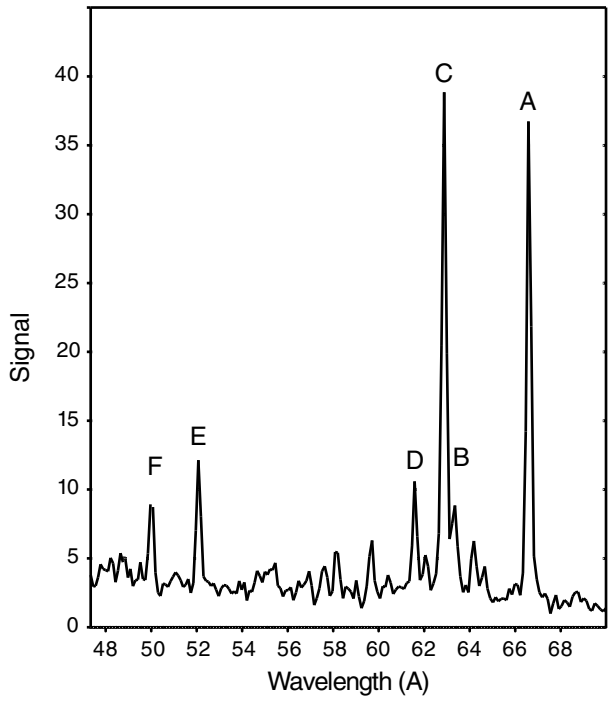

Figure 4. Section of a Xe spectrum obtained at an electron beam ion trap [10]. The spectrometer has a similar Rowland circle diameter (R=5 m) as the one used for the beam-foil spectra shown in figures 1 to 3, but a four times higher groove density. The gain in spectral resolving power is striking. The principal spectral features in this spectrum are identified in table 7.